HHS Public Access

Author manuscript

Cell. Author manuscript; available in PMC 2016 June 04.

Published in final edited form as:

Cell. 2015 June 4; 161(6): 1345–1360. doi:10.1016/j.cell.2015.04.048.

RUNX3 controls a metastatic switch in pancreatic ductal adenocarcinoma

Martin C. Whittle[1], **Kamel Izeradjene**[1], **P. Geetha Rani**[1], **Libing Feng**[1], **Markus A. Carlson**[1], **Kathleen E. DelGiorno**[1], **Laura D. Wood**[2], **Michael Goggins**[2], **Ralph H. Hruban**[2], **Amy E. Chang**[1], **Philamer Calses**[1], **Shelley M. Thorsen**[1], and **Sunil R. Hingorani**[1,3,4,*]

[1]Clinical Research Division, Fred Hutchinson Cancer Research Center, Seattle, WA, 98109

[2]Departments of Pathology and Oncology, Johns Hopkins Medical Institutions, Baltimore, MD, 21231

[3]Public Health Sciences Division, Fred Hutchinson Cancer Research Center, Seattle, WA, 98109

[4] Department of Medicine, Division of Medical Oncology, University of Washington School of Medicine, Seattle, WA, 98195

SUMMARY

For the majority of patients with pancreas cancer, the high metastatic proclivity is life-limiting. Some patients, however, present with and succumb to locally destructive disease. A molecular understanding of these distinct disease manifestations can critically inform patient management. Using genetically engineered mouse models, we show that heterozygous mutation of Dpc4/Smad4 attenuates the metastatic potential of KrasG12D/+;Trp53R172H/+ pancreatic ductal adenocarcinomas while increasing their proliferation. Subsequent loss of heterozygosity of Dpc4 restores metastatic competency while further unleashing proliferation, creating a highly lethal combination. Expression levels of Runx3 respond to and combine with Dpc4 status to coordinately regulate the balance between cancer cell division and dissemination. Runx3 serves as both a tumor suppressor and promoter in slowing proliferation while orchestrating a metastatic program to stimulate cell migration, invasion and secretion of proteins that favor distant colonization. These findings suggest a model to anticipate likely disease behaviors in patients and tailor treatment strategies accordingly.

*Correspondence: Sunil R. Hingorani, MD, PhD, Fred Hutchinson Cancer Research Center, 1100 Fairview Ave N., M5-C800, Seattle, WA 98109-1024, srh@fhcrc.org.

SUPPLEMENTAL INFORMATION

The Supplemental Information includes six Supplemental Figures, three Supplemental Tables and Extended Experimental Procedures.

INTRODUCTION

Patients with carcinomas die primarily of metastatic disease. This is especially true of pancreatic ductal adenocarcinoma (PDA) which is notorious for its early and extreme penchant for metastatic spread. A minority of patients instead present with and succumb to locally advanced disease, although the reasons for these distinct presentations remain unknown. PDA has either overtly metastasized or advanced locally beyond the boundaries of surgical resection in most patients at the time of diagnosis; subsequent median survival is approximately 4.5 and 10.6 months, respectively (Hidalgo, 2010). For the fortunate few for whom surgical resection is possible, median survival increases to 2 years but is not durable: survival at 5 years is only 20% and declines to less than 2% at 10 years (Allison et al., 1998). The majority of these post-operative patients also eventually die of metastatic disease suggesting that clinical Stage I tumors are, in fact, already micrometastatic Stage IV.

In a uniformly lethal disease, prognosis per se may be less informative than the ability to predict disease behaviors and likely proximal cause of death in order to inform rational treatment decisions. Indeed, neoadjuvant strategies for early stage PDA were introduced because many patients ultimately die from distant relapse after surgery; addressing this reality with a course of chemotherapy prior to resection can prolong survival, but runs the attendant risk of local tumor growth beyond surgical boundaries and therefore a lost chance for cure. Thus, knowing when to operate or irradiate and when to treat systemically remains unclear.

PDA begins most commonly in precursor lesions termed pancreatic intraepithelial neoplasms (PanIN) that arise in terminal ductules (Hruban et al., 2001). Activating *KRAS* mutations occur early in preinvasive disease and are almost uniformly present (>90%) in invasive PDA. Mutations in *CDKN2A/INK4A* are similarly abundant in invasive disease (>95%) and point mutations in *TP53* are also common (>75%). Loss of *DPC4/SMAD4* expression, the last of the principal genetic events associated with PDA, occurs late in PanIN-to-PDA progression and is seen in approximately 50% of invasive cancers (Iacobuzio-Donahue et al., 2000).

Engineering these cardinal mutations into the murine pancreas has yielded important insights into mechanisms underlying initiation, progression and maintenance of PDA, as well as the non-cell autonomous contributors to disease biology (Perez-Mancera et al., 2012; Stromnes et al., 2014). Collectively, these studies suggest that distinct combinations of tumor suppressor gene mutations can alter the pace, phenotype and prognosis of the resultant invasive disease. For example, concomitant mutations in *p16/p19* (Aguirre et al., 2003) or *Trp53* (Hingorani et al., 2005) hasten progression initiated by oncogenic *Kras* (Hingorani et al., 2003), albeit with distinct characteristics. In the case of biallelic *p16/p19* loss, the primary tumor progresses rapidly, leading to early death and minimal metastatic disease. $Kras^{LSL\text{-}G12D/+}$;$Trp53^{LSL\text{-}R172H/+}$;*Cre* (*KPC*) animals instead succumb from a combination of both primary and metastatic tumor burdens that closely mimics the common presentation in humans. In contrast, heterozygous deletion of *Dpc4/Smad4* in the context of oncogenic $Kras^{G12D}$ expression generates macroscopic cystic precursors known as mucinous cystic neoplasms (MCN) (Izeradjene et al., 2007). Subsequent progression to

invasive PDA occurs through additional spontaneous events including loss of heterozygosity (LOH) of *Dpc4*, but the disease manifests an attenuated metastatic potential. Invasive PDA that arise from MCN in patients also invariably lose *DPC4* expression (Iacobuzio-Donahue et al., 2000) and have a better prognosis than cancers following the more common PanIN-to-PDA route (Matthaei et al., 2011). Thus, perhaps unexpectedly, decreased TGFβ signaling in certain contexts can give rise to less aggressive PDA.

Continuing these investigations into the pathophysiology of distinct genetic and histologic subtypes of PDA, we engineered targeted heterozygous mutation of *Dpc4* with concomitant point-mutant $Trp53^{R172H}$ and oncogenic $Kras^{G12D}$ in the murine pancreas and defined the resulting disease. We describe a biphasic dependency of Runx3 levels on *Dpc4* gene dosage resulting in a rule set to predict and explain three potential disease presentations in patients. The predicted behaviors can, in turn, inform the rational application and timing of local vs. systemic therapies to maximize survival.

RESULTS

Concomitant *Trp53* mutation restores PanIN-to-PDA progression in the context of $Kras^{G12D}$ expression and *Dpc4* deletion

Conditional endogenous expression and deletion of critical genes (Figure S1A) were targeted to the developing murine pancreas using strategies described previously (Hingorani et al., 2003; Hingorani et al., 2005; Izeradjene et al., 2007). We first established that animals with targeted pancreatic expression of point-mutant *p53* and concomitant heterozygous deletion of *Dpc4/Smad4*, in the absence of oncogenic $Kras^{G12D}$, developed and aged normally with unperturbed pancreatic parenchymal architecture and intact exocrine and endocrine synthetic functions (Figure S1B).

To investigate the effects of concomitant *p53* and *Dpc4* mutation on neoplasms initiated by oncogenic *Kras*, $Kras^{LSL\text{-}G12D/+}$;$Trp53^{LSL\text{-}R172H/+}$;$Dpc4^{flox/+}$;$p48^{Cre/+}$ (*KPDC*) quadruple mutant mice were generated and aged until symptomatic. Concomitant heterozygous deletion of *Dpc4* shortened survival compared with $Kras^{LSL\text{-}G12D/+}$;$Trp53^{LSL\text{-}R172H/+}$;$p48^{Cre/+}$ (*KPC*) littermates (Figure 1A). *KPDC* animals developed solid, multinodular tumors similar to those of *KPC* mice (Figures 1B and 1C), albeit much larger (Figures 1D and 1E). Histologic progression in *KPDC* mice followed the classical PanIN-to-PDA and not MCN-to-PDA sequence. Low-grade PanIN were seen in young animals and subsequently progressed to higher grade and then to invasive PDA (Figures 1F-1I). CK-19 expression (Figure 1J) confirmed the ductal epithelial nature of these neoplasms, and alcian blue revealed their abundant cytoplasmic mucin (Figure 1K). The histologic morphology was predominantly glandular (Table S1) and other less common histologies seen in human PDA, including anaplastic and sarcomatoid, were similarly rare in *KPDC* tumors.

Haploinsufficiency of *Dpc4* attenuates the metastatic drive of $Kras^{G12D}$ and $Trp53^{R172H}$

Belying their earlier demise, *KPDC* animals manifested an unexpected and significant decrease in metastatic disease. Their *KPC* littermates developed widely disseminated disease

as described previously (Hingorani et al., 2005), with a heavy macroscopic tumor burden, principally to the liver (53%) and lungs (47%) (Figure 1L). In contrast, only 21% of *KPDC* littermates developed macroscopically evident metastases which were largely confined to the liver (Figure 1L and Table S1). Moreover, as most metastases in *KPDC* mice were microscopic, they did not contribute substantively to overall tumor burden. Thus, the evolution of pancreas cancer in *KPDC* mice is shifted toward a higher primary tumor burden and less metastatic disease.

Genetic progression of *KPDC* PDA

To investigate the basis for the distinct *in vivo* biological behavior of *KPDC* PDA, we purified primary ductal carcinoma cells as previously described (Hingorani et al., 2005; Schreiber et al., 2004). We first confirmed that the purified PDA cells had recombined and activated the conditional $Kras^{LSL\text{-}G12D}$ and $Trp53^{LSL\text{-}R172H}$ alleles, and likewise deleted the *Dpc4* allele (Figures S1C-S1E). Disease progression was invariably accompanied by spontaneous LOH of *Trp53* (Figure S1D), as typically occurs in murine (Hingorani et al., 2005) and human (Scarpa et al., 1993) PDA with point mutations in one *TP53* allele. Invasive *KPDC* PDA cells typically did not undergo LOH of *Dpc4* but instead frequently retained the remaining wild type (WT) allele (Figure S1E) and persistent protein expression (Figure 1M), unlike the spontaneous loss or epigenetic silencing of the second allele that occurs in *KDC* mice during disease progression (Izeradjene et al., 2007). Detectable levels of *Trp53* were observed consistent with point-mutant expression and LOH. *Cdkn2a*/*Ink4a* (*p16*) expression was frequently lost, although that of the contiguous *p19* allele was retained, suggesting specific promoter methylation rather than genomic deletion as the mechanism of silencing (Izeradjene et al., 2007). The loss of *p16* is notable as prior studies of both *KPC* (Hingorani et al., 2005) and $Kras^{LSL\text{-}G12D/+}$;*p16*/$p19^{-/-}$;*Cre* (Bardeesy et al., 2006) animals found no additional loss of other major TSG during disease progression, establishing non-overlapping mutational spectra in the two model systems. Thus, heterozygous mutation of *Dpc4* increases the selection pressure to lose *p16*, underscoring that WT levels of *Dpc4* can be tumor promoting in this context and that the haploinsufficiency of *Dpc4* in inhibiting primary tumor growth also attenuates metastatic potential. The spontaneous progression of PDA with $Kras^{G12D}$, $Trp53^{R172H}$, $Dpc4^{+/-}$ and loss of *p16* encompasses all four cardinal mutations seen in human PDA (Iacobuzio-Donahue et al., 2012; Iacobuzio-Donahue et al., 2000).

Heterozygous loss of *Dpc4* inhibits metastatic behavior induced by $Kras^{G12D}$ and $Trp53^{R172H}$

Functional assays were performed to explore the relative metastatic deficiency of *KPDC* pancreas cancers. First, we found that the epithelial-to-mesenchymal transition (EMT), a program of morphological and molecular changes implicated in the metastatic phenotype, was qualitatively intact in *KPDC* PDA cells. *KPDC* cells developed actin stress fibers in response to TGFβ (Figures 2A and S2A) and down-regulated surface expression of E-cadherin (Figures 2B and S2B). However, they were less likely to separate from each other in response to TGFβ than *KPC* cells and, despite their qualitative ability to undergo EMT, both the basal migration and invasion of *KPDC* cells were significantly impaired (Figures 2C-2E and S2C and S2D). Moreover, whereas TGFβ stimulated *KPC* cells to migrate,

KPDC cell migration was instead either unaffected or further inhibited. *KPC* cells in monolayer culture also readily formed foci in response to TGFβ, whereas *KPDC* cells did not (not shown).

The cellular phenotypes could be interconverted by depleting or overexpressing *Dpc4* in *KPC* or *KPDC* cells, respectively. *Dpc4* depletion in *KPC* cells inhibited their migration and overexpression of *Dpc4* in *KPDC* cells increased theirs (Figures S2E-G). After injection into the circulation, *KPC* cells formed numerous large pleural and parenchymal metastases sufficient to induce respiratory failure, reflecting the metastatic aggressiveness seen in their autochthonous counterpart (Figures 2G and 2H). *KPDC* cells formed far fewer and smaller lung metastases in animals that remained clinically robust at comparable time points (Figures 2F and 2H). Collectively, these studies reveal that both the baseline properties and responses to TGFβ are essentially mirror images in the presence of WT vs. heterozygous loss of *Dpc4*.

Runx3 drives metastasis in PDA

The dramatically different behaviors of *KPC* and *KPDC* carcinomas suggested that comparative expression profiling might provide mechanistic insights. Expression analyses using customized TGFβ-signaling-specific qPCR arrays identified 15 genes that were upregulated at least 2-fold in *KPC* vs. *KPDC* cells and that might therefore represent metastasis-promoting genes (Table S2). *Dpc4* expression was approximately 2-fold higher in *KPC* than *KPDC* cells, confirming the fidelity of the array results. Completely distinguishing itself was *Runx3*, which was upregulated 36-fold in *KPC* cells (Table S2). *Runx3* belongs to a family of runt-related transcription factors involved in development and differentiation of which *Runx1* and *Runx2* are the best characterized (Blyth et al., 2005). The specificity of *Runx3* upregulation was underscored by the lack of significant changes in the other family members (1.2-fold increase for *Runx1* and 1.5-fold for *Runx2*; not shown). *RUNX1* and *RUNX2* have been identified as TSG in hematopoietic malignancies. Its alternate designation as acute myelogenous leukemia 2 (*AML2*) notwithstanding, what little is known about the role of *RUNX3* in malignancy comes primarily from studies of solid tumors, where it has been implicated on both sides of the cancer divide (i.e. as a TSG in some reports and an oncogene in others). Indeed, its specific role in tumorigenesis remains the subject of considerable controversy (for examples, see Ito et al., 2009; Levanon et al., 2011; Levanon et al., 2001; Li et al., 2002, and see below).

Runx3 gene expression and protein levels correlated with metastatic potential (Figures 3A and 3B). In both *KPC* and *KPDC* carcinoma cells, Runx3 was appropriately localized to the nuclear compartment (Figure S3A), albeit at very different levels. Specific IHC for Runx3 revealed no discernible expression in normal pancreatic ducts, islets or acini; scattered lymphocytes, common sites of elevated Runx3 and useful internal controls (Yarmus et al., 2006), showed strong nuclear expression (Figure 3C). As expected, *KPC* tumors had moderate-to-strong nuclear Runx3 expression (Figures 3D and 3E), whereas *KPDC* tumors typically showed very weak expression (Figures 3F and 3G). Preinvasive lesions adjacent to invasive *KPC* carcinomas also lacked Runx3 expression (Figure 3H). *KPC* metastases exhibited strong nuclear Runx3 expression (Figure 3I) and, in *KPDC* mice that did bear

metastases, both these and the primary tumors often expressed high levels of Runx3 (Figures 3J-L). The upregulation of Runx3 as *KPC* PanIN become invasive and metastatic coincides with the apparent requirement for LOH of *p53* and subsequent accumulation of the point-mutant protein (Hingorani et al., 2005). These observations implicate WT p53 – reported to complex with RUNX3 (Yamada et al., 2010) – in suppressing Runx3 or point-mutant p53 in stabilizing Runx3.

Runx3 promotes metastatic seeding and colonization by remodeling the ECM

To further investigate its effects on metastatic potential, we varied *Runx3* expression in independent *KPDC* and *KPC* carcinoma cell lines (Figures S3B and S3C). *Runx3* overexpression greatly increased the basal migration of *KPDC* cells, and silencing *Runx3* inhibited *KPC* cell migration (Figures 3M, S3D and S3E). TGFβ stimulated migration only in the context of high *Runx3* expression. Anchorage-independent growth in soft agar was similarly influenced by changes in *Runx3* expression (not shown). *KPDC-Runx3* cells also readily formed lung metastases in immunocompromised mice (Figures 3N and 3O), an ability virtually absent in control-transfected *KPDC* cells and once again more like baseline *KPC* cells. A trend toward reduced lung metastasis after *Runx3*-knockdown in *KPC* cells was also observed but did not reach statistical significance, perhaps reflecting incomplete *Runx3* silencing (Figures 3P and 3Q).

KPDC cells were unable to efficiently seed metastases even after direct inoculation into the bloodstream. To successfully colonize a distant site, disseminated cells must not only intravasate but also survive in the circulation, extravasate in a target organ, and fashion a niche that supports metastatic growth. We therefore performed focused array profiling for ECM genes comparing the highly metastatic *KPC* and non-metastatic *KPDC* PDA cells. A survey of the top differentially expressed genes revealed several that have been previously implicated in critical ECM functions, promoting local invasiveness and remodeling of the metastatic niche (Psaila and Lyden, 2009) (Table S3). These include matrix Mmps, Timps, Versican, Spp1 and Sparc (Lunardi et al., 2014).

Osteopontin (*SPP1*) is upregulated in human PDA and portends poor prognosis (Poruk et al., 2013). Spp1 protein (Figure 4A) and transcript levels (Table S3) are also significantly upregulated in *KPC* versus *KPDC* PDA cells. We identified two consensus RUNX3-binding sites and two *SMAD*-binding elements in both the human *SPP1* and murine *Spp1* promoter regions and found that the promoter responds to *RUNX3* overexpression (Figure S4A). Overexpression or silencing of *Runx3* in *KPDC* or *KPC* cells, respectively, caused corresponding changes in *Spp1* expression (Figures 4B, 4C, S4B and S4C). As Spp1 is secreted, we therefore tested whether exogenously added Spp1 influenced migration. *KPDC* cell migration increased significantly in the presence of Spp1, an effect reversed by a neutralizing Spp1 antibody, which also significantly reduced basal *KPC* cell migration (Figure 4D). Spp1 promotes migration through binding to integrins and CD44 receptors, which are also upregulated in *KPC* cells (Table S3), and we found that anti-CD44 antibody decreased Spp1-mediated migration compared to IgG-control-treated counterparts (Figure 4D). Finally, if Spp1 secretion is important for distant colonization, then circulating plasma levels should be high in mice with metastases regardless of genotype. Circulating Spp1 was

indeed elevated in the majority of *KPC* mice, and the relatively few *KPDC* mice, that developed significant metastatic disease burdens (Figure 4E).

Some genes in the ECM profile, including the top-ranked one, *Col6a1*, were less familiar (Table S3). COL6A1 binds fibrillar type I collagen (Bonaldo et al., 1990), itself complicit in PDA aggressiveness and dissemination (e.g. Armstrong et al., 2004). COL6A1 is elevated in the circulating proteome of PDA patients (Yu et al., 2009), and we found two *RUNX3* consensus-binding sites in the *COL6A1*/*Col6a1* promoter region (not shown). Little is known, however, about the specific function(s) of this gene in cancer and, in particular, in PDA. We first confirmed that Col6a1 is differentially expressed in *KPC* and *KPDC* cells (Figures 4F and S4D). Overexpression of *Runx3* in *KPDC* cells increased Col6a1 transcript and protein levels (Figures 4G and S4D), whereas *Runx3* silencing in *KPC* cells reduced them (Figures 4H and S4E). We next tested whether Col6a1 could act as an autocrine enabler of dissemination. *KPC* cells secrete higher levels of Col6a1 than *KPDC* cells (Figure 4I), and overexpressing *Col6a1* in *KPDC* cells increased migration and silencing *Col6a1* in *KPC* cells inhibited it (Figures 4J and S4F-I). Thus, in addition to providing a potentially critical component of the three-dimensional architecture of a developing tumor, Col6a1 also appears to directly stimulate cell motility. Finally, overexpression of *Col6a1* in *KPDC* or knockdown in *KPC* cells reversed their respective abilities to seed lung metastases after intravenous injection (Figures 4K and 4L). Overall, these results suggest that *Runx3* serves to both expel the seed and prepare the soil by directly stimulating cell migration and dissemination, and by inducing the expression of a repertoire of proteins that can reengineer the extracellular matrix to enhance distant colonization.

Heterozygous deletion of *Dpc4* increases proliferation in the context of oncogenic $Kras^{G12D}$ and $Trp53^{R172H}$

The increased primary tumor size at the expense of metastatic disease seen in *KPDC* compared with *KPC* PDA could be explained by increased proliferation, decreased apoptosis, or both. Ki-67 expression was significantly increased in *KPDC* versus *KPC* autochthonous tumors and apoptosis was similarly negligible in both contexts (Figures 5A-5E). In culture, *KPDC* PDA cells were more proliferative than *KPC* cells (Figure 5F) and had similarly low apoptotic rates (not shown). *KPDC* cells were also somewhat less sensitive to growth-arrest by TGFβ (Figure 5F). Substantiating its sometime designation as a TSG, silencing *Runx3* in *KPC* cells unleashed proliferation and overexpression of *Runx3* in *KPDC* cells inhibited it (Figures 5G and 5H). We identified multiple consensus Runx3 binding sites in the $p21^{Cip1/WAF1}$ promoter region and confirmed that Runx3 stimulated its expression (Figure 5I), as previously demonstrated in gastric epithelial cells (Chi et al., 2005).

Rare metastasis of *KPDC* PDA requires LOH of *Dpc4*

The above findings prompted an analysis of *Dpc4* status in paired primary tumors and metastases in the few *KPDC* animals that did develop disseminated disease. The primary tumors revealed focal areas of Dpc4 loss, suggesting a potential source for the disseminated cells (Figures 6A and 6B). In addition, a strong inverse correlation was observed between Dpc4 and Runx3 expression in primary tumors and metastases (Figures 6C and 6D):

complete loss of Dpc4 was associated with elevated levels of Runx3, whereas retained Dpc4 corresponded with low-to-undetectable Runx3 (Figure S5A). These observations suggested that completing the loss of *Dpc4* in PDA cells that had undergone a first (heterozygous) "hit" may confer metastatic potential on cells that previously lacked it, perhaps by increasing Runx3.

To directly investigate the effects of homozygous loss of *Dpc4* on autochthonous PDA, we generated and characterized $Kras^{LSL\text{-}G12D/+}$;$Trp53^{LSL\text{-}R172H/+}$;$Dpc4^{flox/flox}$;$p48^{Cre/+}$ (*KPDDC*) quintuple mutant mice. *KPDDC* mice had a median survival of 125 days, significantly shorter than both *KPDC* and *KPC* cohorts (not shown). Large, multinodular pancreas tumors were found to develop from PanIN precursors (Figures S5B and S5C) and were histologically indistinguishable from *KPDC* or *KPC* PDA (Figures S5D and S5E). *KPDDC* primary tumors grew much faster than *KPDC* and *KPC* PDA, as may be expected from complete loss of canonical TGFβ signaling (Figure S5F). In addition, *KPDDC* mice exhibited metastases to the liver and lungs at similar frequencies (73%) to *KPC* mice, a capability reflected in the elevated levels of Runx3 in *KPDDC* primary tumors (Figure S5G) and purified cells (Figure S5H). This combination of unfettered proliferation and potent dissemination explains the rapid demise of *KPDDC* mice and is consistent with the subset of especially aggressive human PDA with a similar mutational profile (Yachida et al., 2012). In keeping with the role of Runx3 in modulating ECM gene expression to promote metastasis, Spp1 and Col6a1 were also elevated in *KPDDC* compared to *KPDC* cells (Figure S5H). Despite their considerable metastatic competency *in vivo*, *KPDDC* cells were nevertheless notably resistant to induction of EMT by TGFβ *in vitro* (Figures 6E and S5I and S5J). Collectively, these findings suggest a biphasic dependency of metastatic potential on *Dpc4* – mirrored in *Runx3* levels – with heterozygous mutation retarding, and subsequent LOH rescuing, the ability to disseminate (Figure 6F).

Multiple inputs regulate *Runx3* levels

In considering how Runx3 levels might be regulated, three pieces of information provided useful starting points: 1) the dramatic fall and rise in Runx3 levels with stepwise loss of Dpc4; 2) the increase in Runx3 levels coordinately with LOH of *p53* in *KPC* PDA progression; and 3) the presence of multiple consensus binding sites for the Runx3 transcription factor in its own promoter. Although the detailed mechanisms behind the complex regulation of Runx3 levels remain to be elucidated, a working model can nevertheless be elaborated from our findings and corroborated experimentally (Figure 6G). First, we hypothesized that WT p53 promotes Runx3 protein degradation and that point-mutant p53 rescues this effect. This predicts therefore that protein stability would be highest in invasive *KPC* cells and that Runx3 stability should otherwise be comparable in *KPDC* and *KPDDC* cells (as both undergo LOH of p53), unless Dpc4 status additionally contributes. We incubated cells in cycloheximide to arrest protein synthesis and followed the kinetics of Runx3 degradation: protein levels were indeed most stable in *KPC* cells, and the already low Runx3 levels in *KPDC* cells dropped even further (Figures S5K and S5L). These findings suggested that homozygous levels of Dpc4 promoted Runx3 synthesis (which would most readily be accomplished at the transcriptional level) and that heterozygous levels were sufficient to promote Runx3 protein degradation. We predicted

therefore that restoring *Dpc4* expression in *KPDC* cells would increase *Runx3* transcript levels and that partial knockdown in *KPC* would decrease them, both of which were observed (Figures S5M and S5N). That the basal protein levels are both elevated and more stable in *KPDDC* than *KPDC* cells is also consistent with this interpretation, but suggests the presence of at least one more input into Runx3 transcription, perhaps Runx3 itself. In this scenario, once the concentration of the Runx3 transcription factor achieves a critical threshold, it further promotes its own transcription. The *Runx3* promoter contains three consensus Runx3 binding sites, prompting us to test this hypothesis directly in reporter assays with increasing amounts of exogenous Runx3 (Figure S5O). As shown, once Runx3 rises above a certain level, it rapidly increases its own transcription.

RUNX3 drives metastasis in human PDA

To determine whether *RUNX3* served similar roles in human pancreas cancer, we first assessed protein levels in a panel of well-characterized human PDA cell lines (Figure 7A). There are wide differences across these extensively passaged cell lines in the mutational status of the principal TSG, and even among multiple reports of a single line (Deer et al., 2010). Moreover, as disease behavior may also reflect the chronologic sequence in which mutations arise (see Izeradjene et al., 2007) and we cannot know that history, we asked whether RUNX3 levels alone could be used to infer metastatic capability. We chose two of the highest (CFPAC-1 and Panc-1) and one of the lowest (MiaPaCa-2) *RUNX3*-expressing lines for further study (Figure 7A). We note that although MiaPaCa-2 cells are WT for *DPC4*, they contain markedly decreased – but not completely absent – levels of TGFβR2 (not shown), suggesting an alternative way to attenuate DPC4-mediated signaling and potentially produce the same functional outcome.

Basal levels of RUNX3 predicted migration, as MiaPaCa-2 cells migrated less well than either CFPAC-1 or Panc-1 cells (Figures 7B and 7C). The respective responses of these cell lines to TGFβ also followed the pattern seen with murine PDA cells: TFGβ modestly inhibited MiaPaCa-2 cell migration, as it did with *KPDC* cells, whereas it promoted or left unaffected the high basal migration of CFPAC-1 and Panc-1 cells, similar to *KPC* cells. Overexpression of *RUNX3* in MiaPaCa-2 cells (Figure S6A) greatly increased migration (Figures 7B and S6B). Conversely, depletion of *RUNX3* in both Panc-1 cells and CFPAC-1 cells inhibited migration (Figures 7C and S6C and S6D). Anchorage-independent growth of MiaPaCa-2 and CFPAC-1 cells was similarly influenced by *RUNX3* overexpression and knockdown, respectively (Figures S6E and S6F). MiaPaCa-2 cells overexpressing *RUNX3* developed a significantly greater metastatic burden after intravenous inoculation into NOD/SCID mice than vector-control cells (Figures 7D and 7E). Conversely, targeted depletion of *RUNX3* in Panc-1 cells diminished their overall metastatic potential. Although both control and *RUNX3*-knockdown Panc-1 cells produced a comparable metastatic burden in the lungs (Figure S6G), the ability to seed and support secondary liver metastases was significantly impaired by *RUNX3* depletion as reflected in the distinct gross pathology (Figure 7F) and liver weights between the two groups: 4.3 +/− 0.6 g (n=4) vs. 0.53 +/− 0.06 g (n=3; $p<0.005$), respectively. *SPP1* and *COL6A1* expression levels were also influenced as expected by modulating *RUNX3* expression in these respective human cell lines, and *COL6A1* overexpression stimulated migration (Figures S6H-S6J). Thus, the *RUNX3*-

dependent metastatic drive and responses to TGFβ observed in human PDA cells paralleled the behaviors of their murine counterparts.

RUNX3 predicts survival and disease behavior in human PDA

Cohorts of PDA patients with evaluable tissue and long-term survival data are rare. Using the available resources, we investigated whether RUNX3 levels in primary tumors influenced disease behavior and survival after surgery and could even predict response to various forms of therapy. Given the predilection for distant relapse after surgery, we hypothesized that high RUNX3 levels in primary PDA epithelial cells might portend poor prognosis. In a cohort of PDA patients who underwent definitive resection (*n*=88), RUNX3 levels did indeed correlate with survival (Figures 7G, S6L and S6M). Since no information was available in this data set on site of relapse, we interrogated a separate annotated cohort assembled by The International Cancer Genome Consortium (ICGC) that included whole-tissue transcriptome analyses and data on relapse pattern and survival after surgery. In this case, *RUNX3* transcript levels did not correlate with either survival or relapse site, an unsurprising result given that PDA are dominated by inflammatory cells with high baseline *RUNX3* levels, and whole tissue preparations from biopsies would inevitably include transcripts from all cell populations. We instead assessed the downstream targets of epithelial *RUNX3* expression and found elevated tissue levels of *SPP1* and *COL6A1* in patients who developed distant as opposed to local disease recurrence after surgery (Figure 7H).

As a final measure of potentially actionable information contained in RUNX3 levels, we investigated whether they could help inform the choice and sequencing of different treatment modalities in the post-operative and, by extension, pre-operative settings. We reasoned that patients with lower levels of RUNX3 might respond better to radiotherapy, given the higher risk of local relapse, whereas patients with high RUNX3 might fare better with systemic therapy. As predicted, the use of local radiation favored patients with low RUNX3 (Figure 7I). Conversely, patients with high RUNX3 benefitted most from systemic treatment whereas those with low RUNX3 did not (and may even have been harmed given that low RUNX3 should otherwise portend a better prognosis). These analyses support the idea that RUNX3 levels in the primary tumor may help inform the management of pancreas cancer patients.

DISCUSSION

We systematically varied *Dpc4/Smad4* gene dosage in $Kras^{G12D/+};Trp53^{R172H/+};p48^{Cre/+}$ (*KPC*) PDA recapitulating the spectrum of disease presentations encountered in patients and identified the *Runx3/RUNX3* transcription factor as the convergence point for several inputs that ultimately govern the balance between cell division and dissemination. *RUNX3* slows the proliferation of PDA cells while endowing them with the ability to both migrate to and participate in the construction of the metastatic niche by secreting critical stromal matrix constituents. These findings suggest additional therapeutic targets in pancreas cancer and have the potential to inform clinical decision-making at key junctures in disease management.

Balancing proliferation and dissemination in PDA

The cellular demands of proliferation and dissemination appear to compete in pancreas cancers, at least until *Dpc4* signaling is completely lost. Our data suggest that partial attenuation of TGFβ signaling shifts the burden of disease toward primary tumor growth by lowering barriers to proliferation at the expense of sacrificing mediators of metastasis. Governing this switch is the transcription factor *Runx3*, which integrates inputs from *Dpc4* and *Trp53* (Figure 6G) to generate three broad sets of biological behavior. These shifts in pathobiology with mutational state also help explain patterns of spread observed in patients. At one extreme are patients with locally invasive and destructive tumors and minimal discernible dissemination; at the other are patients with a more restricted primary tumor but widespread metastases. Complete loss of *Dpc4* in the context of point mutant *Trp53* reveals a third state: uninhibited primary tumor growth together with high metastatic potential.

It may seem paradoxical that diminution of *Dpc4* signaling can impede dissemination, given that loss of expression frequently, though not always (Iacobuzio-Donahue et al., 2009), occurs in PDA metastases. However, the precise levels of signaling appear to be critically important. Approximately half of conventional PDA lose expression of *DPC4/SMAD4* and this is thought to represent a late event (Wilentz et al., 2000). As these data are derived from IHC observations, they are generally bimodal (i.e. all or none) and cannot reliably report heterozygous loss of *DPC4*. In autopsy series of PDA patients, a range of metastatic disease burdens has been observed, with death not infrequently attributable to local destruction as opposed to disseminated disease (Iacobuzio-Donahue et al., 2009). Two distinct patterns of metastatic spread emerge: widely metastatic disease characteristic of the majority of cases and an oligometastatic state in a minority. In light of our findings, the most aggressive disease presentation plausibly involves heterozygous mutation of *DPC4* relatively early in disease progression, promoting aggressive local growth and invasion; subsequent loss of *DPC4* expression from the remaining allele in a subclone would then give rise to a highly metastatic subpopulation. Indeed, in the few *KPDC* animals that showed metastatic disease, the tumor cells in those metastases had frequently lost *Dpc4* expression. In this setting, survival would be threatened by the sequelae of both local and disseminated disease burdens in a highly lethal combination.

Resolving conflicting roles of *RUNX3* in tumor progression

RUNX3 has previously been proposed as both promoting and suppressing cancer progression, and sometimes ascribed contradictory roles in the same cancer. Although several studies point toward a tumor suppressive role for RUNX3 (e.g. Bae and Choi, 2004; Lee et al., 2013), a small number of reports indicate that its oncogenic activity might extend beyond murine lymphomas to include basal cell, skin, head and neck, and ovarian cancers (Chuang and Ito, 2010). In gastric carcinoma, *RUNX3* has been identified as both a TSG (e.g. Li et al., 2002) and an oncogene (e.g. Levanon et al., 2011). The controversy notwithstanding, these studies may in fact reflect a multifaceted role for *RUNX3* signaling, consistent with the dual and context-dependent role of TGFβ signaling as a whole. We propose that *RUNX3* indeed functions as both tumor suppressor and promoter, depending not only on the genetic and cellular contexts but also on the specific behavior in question, namely, primary tumor growth or metastatic spread.

EMT and disease dissemination: an imperfect relationship

Both highly metastatic (*KPC*) and poorly metastatic (*KPDC*) PDA cells manifested the classic phenotypic and molecular features of EMT in response to TGFβ. Epithelial cells from highly metastatic *KPDDC* tumors, on the other hand, were resistant to EMT and remained in close contact with each other. Thus, attempting to extrapolate the potential to metastasize *in vivo* from the ability to morph *in vitro* seems tenuous at best. Indeed, despite its intuitive appeal as the malignant mimic of the cellular plasticity required during embryogenesis, positing the EMT as an essential feature of the metastatic program remains controversial (Tarin et al., 2005). The considerable *in vitro* data in support of the concept are counterbalanced by a lack of *in vivo* evidence in autochthonous human cancers. Our data suggest that if EMT does occur, it is not the only means by which metastases can develop, at least not in pancreas cancer. *RUNX3* may promote distinct, perhaps overlapping, metastatic programs involving the dissemination of both single cells and groups or clusters of cells, a possibility first considered over four decades ago (Fidler, 1973) and revisited more recently (Friedl and Alexander, 2011). As a principal cause of cancer mortality, understanding the basis for and learning how to inhibit metastasis are of more than academic interest. Current efforts to target specific features of EMT as a strategy for disrupting dissemination may be incomplete, and the model systems developed and described here revealing distinct metastatic programs may prove fruitful in future investigations.

Local growth vs. disseminated disease: therapeutic implications

The unusual ability of PDA to spread has spurred efforts to advance systemic neoadjuvant therapies and address at the outset the almost inevitable and frequently rapid appearance of metastases. This strategy is not without risks: beyond the potential toxicities looms the possibility that a previously contained tumor will breach the immediate confines of resectability. Indeed, a minority of early stage (I/II) or locally advanced (Stage III) tumors are destined to remain local; these patients can often be managed for many months with no overt evidence of dissemination. In such patients, treating with chemotherapy first and delaying surgery may forfeit the rare window to operate. In a large meta-analysis of over 4,000 early stage pancreas cancer patients who received some form of neoadjuvant therapy, fully 30% became inoperable during the course of treatment (Gillen et al., 2010). The ideal types, timing, duration and sequence of adjuvant chemotherapy and radiotherapy are also unclear, with the role of radiation being especially contentious (Katz et al., 2010). Conflicting results in the setting of complex trial designs have confounded meaningful comparisons and precluded consensus on how best to incorporate distinct modalities into PDA management.

Taking the specific case of early-stage disease as an example, distinguishing those patients to treat with neoadjuvant therapy from those to resect immediately remains especially challenging. The studies presented here suggest that *RUNX3* may help inform such decisions, particularly when interpreted in the context of *DPC4* status (Figure 7J). High levels of RUNX3 increase the migratory and metastatic potential of both murine and human PDA cells which, in the context of intact *DPC4*, defines the most likely cause of death. These patients would likely benefit most from initial systemic therapy followed by resection given the comparatively lower risk for local growth. Patients with resectable disease and low

RUNX3 levels benefit less from systemic treatment up-front and should instead be resected (or treated with a short course of radiation prior to resection, if needed). Patients with high RUNX3 and complete loss of *DPC4* pose the greatest challenge: if neoadjuvant therapy is attempted at all, it may make sense to invert the normal sequence and give a short course of chemoradiation to achieve some local control prior to systemic cytotoxics; however, the primary tumor must be followed closely so as not to lose the opportunity for a definitive resection. Alternatively, combining systemic therapy with cell cycle inhibitors may allow treatment of occult disseminated disease while minimizing the risks of local tumor growth. These admittedly speculative hypotheses nevertheless suggest a framework for future studies that will ultimately provide the measure of their merit.

EXPERIMENTAL PROCEDURES

Mouse Strains

All animal studies were approved by the Institutional Animal Care and Use Committee of the Fred Hutchinson Cancer Research Center. Conditional $Trp53^{LSL\text{-}R172H/+}$, $Dpc4^{flox/+}$, $Kras^{LSL\text{-}G12D/+}$, and $p48^{Cre/+}$ mice strains described earlier (Hingorani et al., 2003; Hingorani et al., 2005; Izeradjene et al., 2007) were interbred to obtain $Kras^{LSL\text{-}G12D/+}$;$Trp53^{LSL\text{-}R172H/+}$;$Dpc4^{flox/+}$;$p48^{Cre/+}$ (*KPDC*),$Kras^{LSL\text{-}G12D/+}$;$Trp53^{LSL\text{-}R172H/+}$;$Dpc4^{flox/+}$;$p48^{Cre/+}$ (*KPC*), and various littermate control animals on a mixed background. Nude mice (Athymic NCr-nu/nu, NCI Frederick USA) and NOD.SCID/NCr mice (CCEH Specialized Mouse Services, FHCRC) were used in pulmonary metastasis assays.

Histology and immunohistochemistry

Tissues were fixed in 10% neutral buffered formalin, embedded in paraffin and 5 μm sections were prepared. Routine H&E and immunohistochemistry (IHC) were performed as previously described (Hingorani et. al., 2003) and IHC scoring was done blinded. Biotinylated secondary antibody and the Elite vectastain kit (Vector Lab, CA, USA) were used for signal detection and DAB was used as a chromogen substrate. Primary antibodies: amylase (1:800, Sigma, Chicago, IL, USA); CK-19 (DakoCytomation, Denmark); cleaved caspase 3 (1:100, Biocare, CA, USA); Dpc4 (1:300, Abcam, MA, USA); insulin (1:200, Dako, CA, USA); Ki-67 (1:25, Dako, CA, USA); and Runx3 (1:200 for murine and 1:100 for human IHC, Cell Signaling, MA, USA).

Assessment of primary and metastatic disease burden

Complete necropsies were performed on all study animals. Gross pathology and histopathology of all internal organs were analyzed for macroscopic and microscopic disease, respectively. Primary (1°) histology was defined as representing ≥ 50% assessed tissue; secondary (2°) histology involved >25% but <50%.

Statistical analyses

Unless otherwise indicated, the significance of data was determined by the Student's *t*-test (two-tailed) for all *in vitro* studies. A value of $p<0.05$ was deemed significant. Fisher's exact

t-test was performed for comparison of metastatic disease burdens in *KPC* vs. *KPDC* cohorts. All statistical analyses were performed using GraphPad Prism 6.0 software.

Additional experimental details can be found in Extended Experimental Procedures.

Supplementary Material

Refer to Web version on PubMed Central for supplementary material.

ACKNOWLEDGEMENTS

We thank past and present members of the Hingorani Laboratory for technical assistance and helpful discussions. We thank John D. Potter for comments on the manuscript. We are grateful to Fiona Pakiam for histotechnical support and to Nathan Lee for assistance with figure preparation. We apologize to colleagues for our inability to cite many primary references due to space constraints. This work was supported by NCI grants CA129537, CA161112 and CA114028 to S.R.H, CA62924 and support from Sol Goldman Pancreatic Cancer Research Center to L.D.W, M.G. and R.H.H., and support to S.R.H from the Giles W. and Elise G. Mead Foundation, the National Pancreas Foundation and David Jones and Maryanne Tagney-Jones.

REFERENCES

Aguirre AJ, Bardeesy N, Sinha M, Lopez L, Tuveson DA, Horner J, Redston MS, DePinho RA. Activated Kras and Ink4a/Arf deficiency cooperate to produce metastatic pancreatic ductal adenocarcinoma. Genes Dev. 2003; 17:3112–3126. [PubMed: 14681207]

Allison DC, Piantadosi S, Hruban RH, Dooley WC, Fishman EK, Yeo CJ, Lillemoe KD, Pitt HA, Lin P, Cameron JL. DNA content and other factors associated with ten-year survival after resection of pancreatic carcinoma. J Surg Oncol. 1998; 67:151–159. [PubMed: 9530884]

Armstrong T, Packham G, Murphy LB, Bateman AC, Conti JA, Fine DR, Johnson CD, Benyon RC, Iredale JP. Type I collagen promotes the malignant phenotype of pancreatic ductal adenocarcinoma. Clin Cancer Res. 2004; 10:7427–7437. [PubMed: 15534120]

Bae SC, Choi JK. Tumor suppressor activity of RUNX3. Oncogene. 2004; 23:4336–4340. [PubMed: 15156190]

Bardeesy N, Aguirre AJ, Chu GC, Cheng KH, Lopez LV, Hezel AF, Feng B, Brennan C, Weissleder R, Mahmood U, et al. Both p16(Ink4a) and the p19(Arf)-p53 pathway constrain progression of pancreatic adenocarcinoma in the mouse. Proc Natl Acad Sci U S A. 2006; 103:5947–5952. [PubMed: 16585505]

Blyth K, Cameron ER, Neil JC. The RUNX genes: gain or loss of function in cancer. Nat Rev Cancer. 2005; 5:376–387. [PubMed: 15864279]

Bonaldo P, Russo V, Bucciotti F, Doliana R, Colombatti A. Structural and functional features of the alpha 3 chain indicate a bridging role for chicken collagen VI in connective tissues. Biochemistry. 1990; 29:1245–1254. [PubMed: 2322559]

Chi XZ, Yang JO, Lee KY, Ito K, Sakakura C, Li QL, Kim HR, Cha EJ, Lee YH, Kaneda A, et al. RUNX3 suppresses gastric epithelial cell growth by inducing p21(WAF1/Cip1) expression in cooperation with transforming growth factor {beta}-activated SMAD. Molecular and cellular biology. 2005; 25:8097–8107. [PubMed: 16135801]

Chuang LS, Ito Y. RUNX3 is multifunctional in carcinogenesis of multiple solid tumors. Oncogene. 2010; 29:2605–2615. [PubMed: 20348954]

Deer EL, Gonzalez-Hernandez J, Coursen JD, Shea JE, Ngatia J, Scaife CL, Firpo MA, Mulvihill SJ. Phenotype and genotype of pancreatic cancer cell lines. Pancreas. 2010; 39:425–435. [PubMed: 20418756]

Fidler IJ. The relationship of embolic homogeneity, number, size and viability to the incidence of experimental metastasis. European journal of cancer. 1973; 9:223–227. [PubMed: 4787857]

Friedl P, Alexander S. Cancer invasion and the microenvironment: plasticity and reciprocity. Cell. 2011; 147:992–1009. [PubMed: 22118458]

Gillen S, Schuster T, Meyer Zum Buschenfelde C, Friess H, Kleeff J. Preoperative/neoadjuvant therapy in pancreatic cancer: a systematic review and meta-analysis of response and resection percentages. PLoS medicine. 2010; 7:e1000267. [PubMed: 20422030]

Hidalgo M. Pancreatic cancer. The New England journal of medicine. 2010; 362:1605–1617. [PubMed: 20427809]

Hingorani SR, Petricoin EF, Maitra A, Rajapakse V, King C, Jacobetz MA, Ross S, Conrads TP, Veenstra TD, Hitt BA, et al. Preinvasive and invasive ductal pancreatic cancer and its early detection in the mouse. Cancer Cell. 2003; 4:437–450. [PubMed: 14706336]

Hingorani SR, Wang L, Multani AS, Combs C, Deramaudt TB, Hruban RH, Rustgi AK, Chang S, Tuveson DA. Trp53R172H and KrasG12D cooperate to promote chromosomal instability and widely metastatic pancreatic ductal adenocarcinoma in mice. Cancer Cell. 2005; 7:469–483. [PubMed: 15894267]

Hruban RH, Adsay NV, Albores-Saavedra J, Compton C, Garrett ES, Goodman SN, Kern SE, Klimstra DS, Kloppel G, Longnecker DS, et al. Pancreatic intraepithelial neoplasia: a new nomenclature and classification system for pancreatic duct lesions. Am J Surg Pathol. 2001; 25:579–586. [PubMed: 11342768]

Iacobuzio-Donahue CA, Fu B, Yachida S, Luo M, Abe H, Henderson CM, Vilardell F, Wang Z, Keller JW, Banerjee P, et al. DPC4 gene status of the primary carcinoma correlates with patterns of failure in patients with pancreatic cancer. J Clin Oncol. 2009; 27:1806–1813. [PubMed: 19273710]

Iacobuzio-Donahue CA, Velculescu VE, Wolfgang CL, Hruban RH. Genetic basis of pancreas cancer development and progression: insights from whole-exome and whole-genome sequencing. Clin Cancer Res. 2012; 18:4257–4265. [PubMed: 22896692]

Iacobuzio-Donahue CA, Wilentz RE, Argani P, Yeo CJ, Cameron JL, Kern SE, Hruban RH. Dpc4 protein in mucinous cystic neoplasms of the pancreas: frequent loss of expression in invasive carcinomas suggests a role in genetic progression. Am J Surg Pathol. 2000; 24:1544–1548. [PubMed: 11075857]

Ito K, Inoue KI, Bae SC, Ito Y. Runx3 expression in gastrointestinal tract epithelium: resolving the controversy. Oncogene. 2009; 28:1379–1384. [PubMed: 19169278]

Izeradjene K, Combs C, Best M, Gopinathan A, Wagner A, Grady WM, Deng CX, Hruban RH, Adsay NV, Tuveson DA, et al. Kras(G12D) and Smad4/Dpc4 haploinsufficiency cooperate to induce mucinous cystic neoplasms and invasive adenocarcinoma of the pancreas. Cancer Cell. 2007; 11:229–243. [PubMed: 17349581]

Katz MH, Fleming JB, Lee JE, Pisters PW. Current status of adjuvant therapy for pancreatic cancer. The oncologist. 2010; 15:1205–1213. [PubMed: 21045189]

Lee YS, Lee JW, Jang JW, Chi XZ, Kim JH, Li YH, Kim MK, Kim DM, Choi BS, Kim EG, et al. Runx3 inactivation is a crucial early event in the development of lung adenocarcinoma. Cancer Cell. 2013; 24:603–616. [PubMed: 24229708]

Levanon D, Bernstein Y, Negreanu V, Bone KR, Pozner A, Eilam R, Lotem J, Brenner O, Groner Y. Absence of Runx3 expression in normal gastrointestinal epithelium calls into question its tumour suppressor function. EMBO molecular medicine. 2011; 3:593–604. [PubMed: 21786422]

Levanon D, Brenner O, Negreanu V, Bettoun D, Woolf E, Eilam R, Lotem J, Gat U, Otto F, Speck N, et al. Spatial and temporal expression pattern of Runx3 (Aml2) and Runx1 (Aml1) indicates non-redundant functions during mouse embryogenesis. Mechanisms of development. 2001; 109:413–417. [PubMed: 11731260]

Li QL, Ito K, Sakakura C, Fukamachi H, Inoue K, Chi XZ, Lee KY, Nomura S, Lee CW, Han SB, et al. Causal relationship between the loss of RUNX3 expression and gastric cancer. Cell. 2002; 109:113–124. [PubMed: 11955451]

Lunardi S, Muschel RJ, Brunner TB. The stromal compartments in pancreatic cancer: are there any therapeutic targets? Cancer letters. 2014; 343:147–155. [PubMed: 24141189]

Matthaei H, Schulick RD, Hruban RH, Maitra A. Cystic precursors to invasive pancreatic cancer. Nature reviews Gastroenterology & hepatology. 2011; 8:141–150.

Perez-Mancera PA, Guerra C, Barbacid M, Tuveson DA. What we have learned about pancreatic cancer from mouse models. Gastroenterology. 2012; 142:1079–1092. [PubMed: 22406637]

Poruk KE, Firpo MA, Scaife CL, Adler DG, Emerson LL, Boucher KM, Mulvihill SJ. Serum osteopontin and tissue inhibitor of metalloproteinase 1 as diagnostic and prognostic biomarkers for pancreatic adenocarcinoma. Pancreas. 2013; 42:193–197. [PubMed: 23407481]

Psaila B, Lyden D. The metastatic niche: adapting the foreign soil. Nat Rev Cancer. 2009; 9:285–293. [PubMed: 19308068]

Scarpa A, Capelli P, Mukai K, Zamboni G, Oda T, Iacono C, Hirohashi S. Pancreatic adenocarcinomas frequently show p53 gene mutations. The American journal of pathology. 1993; 142:1534–1543. [PubMed: 8494051]

Schreiber FS, Deramaudt TB, Brunner TB, Boretti MI, Gooch KJ, Stoffers DA, Bernhard EJ, Rustgi AK. Successful growth and characterization of mouse pancreatic ductal cells: functional properties of the Ki-RAS(G12V) oncogene. Gastroenterology. 2004; 127:250–260. [PubMed: 15236190]

Stromnes IM, DelGiorno KE, Greenberg PD, Hingorani SR. Stromal reengineering to treat pancreas cancer. Carcinogenesis. 2014; 35:1451–1460. [PubMed: 24908682]

Tarin D, Thompson EW, Newgreen DF. The fallacy of epithelial mesenchymal transition in neoplasia. Cancer Res. 2005; 65:5996–6000. discussion 6000-5991. [PubMed: 16024596]

Wilentz RE, Iacobuzio-Donahue CA, Argani P, McCarthy DM, Parsons JL, Yeo CJ, Kern SE, Hruban RH. Loss of expression of Dpc4 in pancreatic intraepithelial neoplasia: evidence that DPC4 inactivation occurs late in neoplastic progression. Cancer Res. 2000; 60:2002–2006. [PubMed: 10766191]

Yachida S, White CM, Naito Y, Zhong Y, Brosnan JA, Macgregor-Das AM, Morgan RA, Saunders T, Laheru DA, Herman JM, et al. Clinical significance of the genetic landscape of pancreatic cancer and implications for identification of potential long-term survivors. Clin Cancer Res. 2012; 18:6339–6347. [PubMed: 22991414]

Yamada C, Ozaki T, Ando K, Suenaga Y, Inoue K, Ito Y, Okoshi R, Kageyama H, Kimura H, Miyazaki M, et al. RUNX3 modulates DNA damage-mediated phosphorylation of tumor suppressor p53 at Ser-15 and acts as a co-activator for p53. The Journal of biological chemistry. 2010; 285:16693–16703. [PubMed: 20353948]

Yarmus M, Woolf E, Bernstein Y, Fainaru O, Negreanu V, Levanon D, Groner Y. Groucho/transducin-like Enhancer-of-split (TLE)-dependent and -independent transcriptional regulation by Runx3. Proc Natl Acad Sci U S A. 2006; 103:7384–7389. [PubMed: 16651517]

Yu KH, Barry CG, Austin D, Busch CM, Sangar V, Rustgi AK, Blair IA. Stable isotope dilution multidimensional liquid chromatography-tandem mass spectrometry for pancreatic cancer serum biomarker discovery. J Proteome Res. 2009; 8:1565–1576. [PubMed: 19199705]

Highlights

- Dpc4 dosage regulates Runx3 levels in a biphasic manner
- Runx3 controls the balance between local growth and dissemination in PDA
- Runx3 functions as both tumor suppressor and tumor promoter in PDA
- Dpc4 and Runx3 levels can jointly inform clinical decision-making

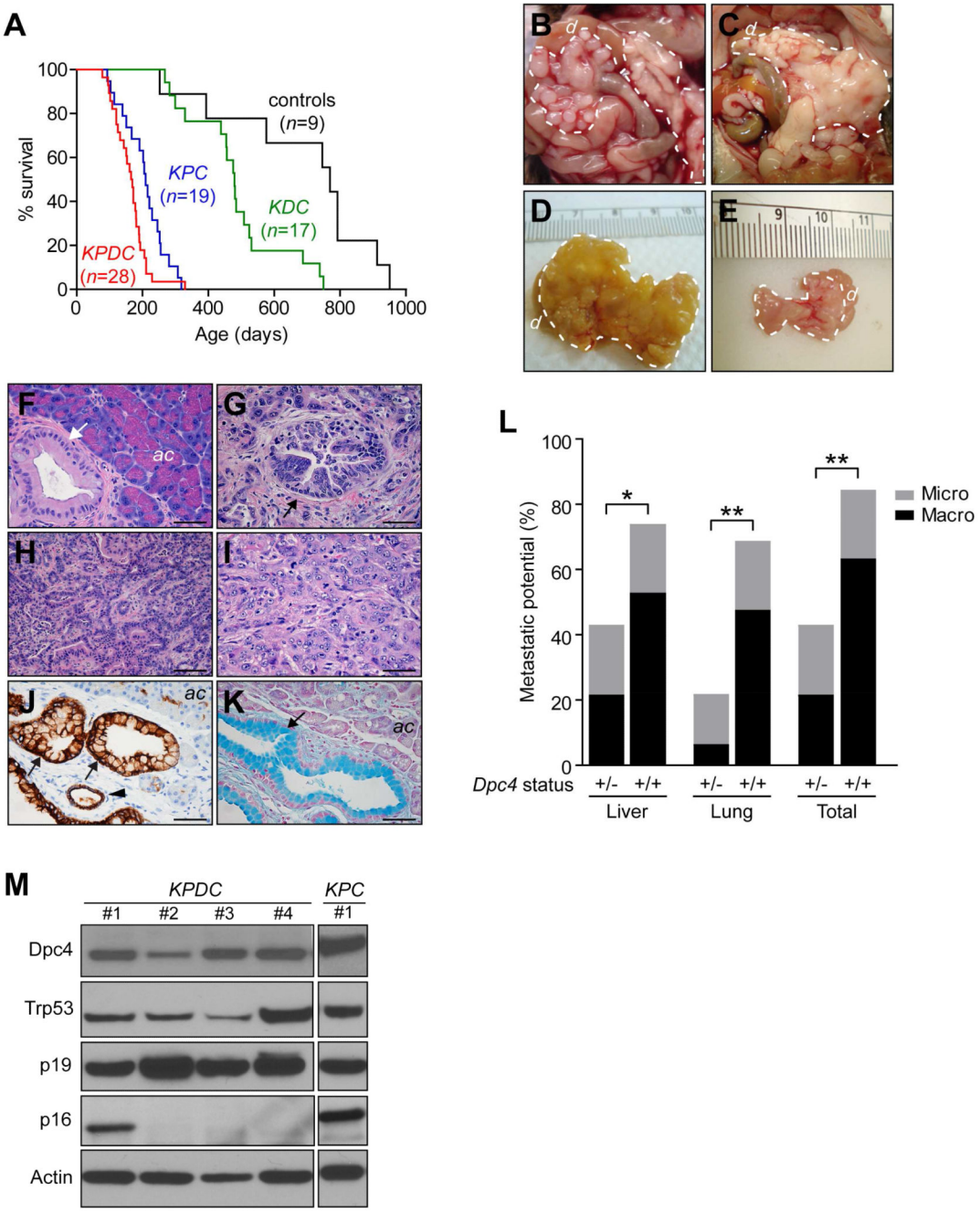

Figure 1. Molecular characterization of tumor progression in *KPDC* mice

(A) Kaplan-Meier survival of *KPDC* animals (167 days) was significantly less than control animals (769 days, p<0.001), $Kras^{LSL\text{-}G12D/+}$;$Dpc4^{flox/+}$;$p48^{Cre/+}$ (*KDC*) mice (479 days, p<0.001) and *KPC* mice (209 days, p<0.05) (log rank test for each pairwise combination).

(B and C) Gross pathology of *KPDC* pancreata at necropsy. Dashed lines, tumor.

(D) Representative *KPDC* tumor.

(E) Representative *KPC* tumor.

(F) Pancreas histology in young *KPDC* animal (age = 109 days). Arrow, PanIN-1A.

(G) Pancreas histology in older *KPDC* animal (age = 165 days). Arrow, PanIN-3.
(H) Moderately well-differentiated *KPDC* PDA.
(I) Poorly differentiated *KPDC* PDA.
(J) CK-19 immunoreactivity highlights *KPDC* ductal epithelium. Arrows, PanIN-1A; arrowhead, normal duct.
(K) Alcian blue histochemistry (arrow) reveals mucin content in preinvasive *KPDC* lesion.
(L) Metastatic potential (% with metastases) in *KPDC* (+/−) and *KPC* (+/+) animals (*p<0.05, **p<0.01). (+/+) and (+/−) indicate WT and heterozygous deleted *Dpc4*, respectively.
(M) Immunoblots of representative *KPDC* and *KPC* primary PDA cell lysates from independent animals.
d, duodenum; *ac*, acinar cells. Scale bars, 50 μm. See also Table S1 and Figure S1.

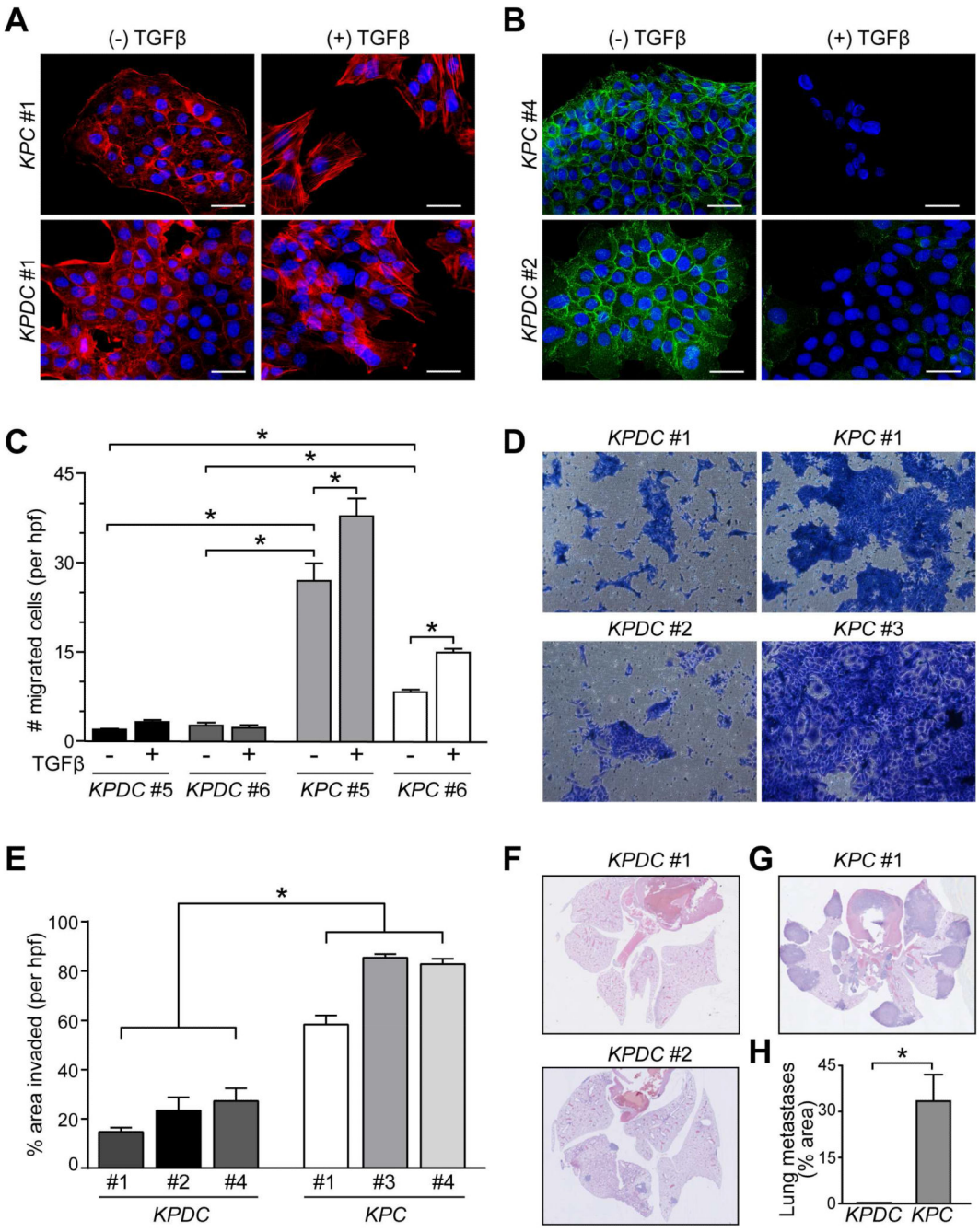

Figure 2. Dpc4 status affects morphologic and cellular behaviors associated with metastasis

(A and B) Immunofluorescence of actin stress fibers (A) and surface E-cadherin (B) in representative *KPC* and *KPDC* PDA cells ±TGFβ. Nuclei are counterstained with DAPI (blue). Scale bars, 50 μm.

(C) Cell migration of representative *KPC* and *KPDC* primary PDA cells from 3 independent experiments (mean ± SEM; *p<0.0001).

(D and E) Representative images (D) and quantification (E) of *KPDC* and *KPC* cells after invasion through Matrigel (n=6 wells per cell line, *p<0.005).

(F-H) Representative images (F and G) and quantification (H) of pulmonary metastases after i.v. inoculation. Two different levels from three injected animals each were assessed (mean ± SEM; *p<0.05). See also Figure S2.

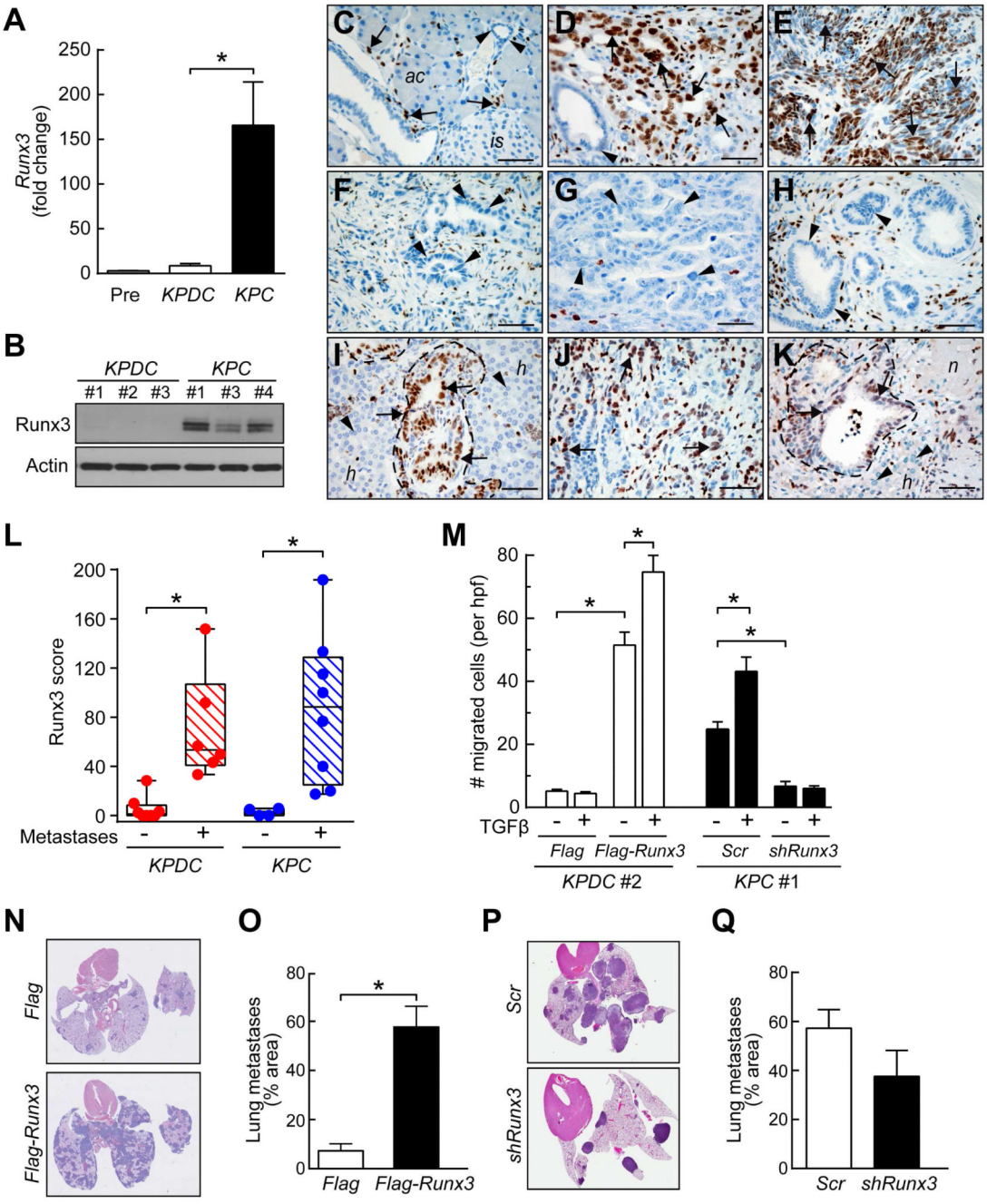

Figure 3. Runx3 promotes metastasis in murine PDA

(A) *Runx3* qRT-PCR in *KC* preinvasive (Pre) and *KPDC* and *KPC* invasive PDA cells (n=4-5 each; mean ± SEM; *p=0.05).

(B) Runx3 immunoblots in representative *KPDC* and *KPC* PDA cells. Actin, loading control.

(C) Runx3 expression in normal pancreas. Arrows, lymphocytes; arrowheads, duct; *ac*, acini; *is*, islet.

(D) Runx3 expression in undifferentiated region of invasive *KPC* PDA (arrows). Arrowhead, PanIN-1A.
(E) Runx3 expression in sarcomatoid region of invasive *KPC* PDA (arrows).
(F and G) Absence of Runx3 in carcinoma cells of two different *KPDC* PDA (arrowheads).
(H) PanIN in *KPC* animals lack Runx3 expression (arrowheads).
(I) Runx3 expression (arrows) in *KPC* liver metastases (outline) from primary PDA in panel (E); adjacent hepatocytes (*h*) lack Runx3 (arrowheads).
(J) Runx3 expression (arrows) in region of primary PDA from *KPDC* animal that developed metastases.
(K) Runx3 expression (arrows) in *KPDC* liver metastasis from primary PDA in (J) and lack of Runx3 (arrowheads) in adjacent hepatocytes (*h*). *n*, area of necrosis.
(L) Runx3 expression in *KPDC* and *KPC* primary tumors. Each point represents mean of three hpf from an independent animal (*$p<0.05$).
(M) Cell migration ±TGFβ in representative *KPDC* cells with (*Flag-Runx3*) or without (*Flag*) *Runx3* overexpression, and in,*KPC* cells with (*shRunx3*) or without (*Scr*) *Runx3* depletion. Data represent three independent experiments (mean ± SEM; *$p<0.01$).
(N and O) Representative lung sections (N) and quantification (O) of pulmonary metastases in mice injected with control (*Flag*) or *Runx3*-overexpressing (*Flag-Runx3*) *KPDC*#1 cells. Two different histological levels from a total of three injected animals for each condition were assessed (mean ± SEM; *$p<0.005$).
(P and Q) Representative lung sections (P) and quantification (Q) of pulmonary metastases in mice injected with control (*Scr*) or Runx3-depleted (*shRunx3*) *KPC*#1 cells. Two different histological levels from a total of three injected animals each were assessed (mean ± SEM; $p=0.21$).
Scale bars, 50 μm. See also Figure S3.

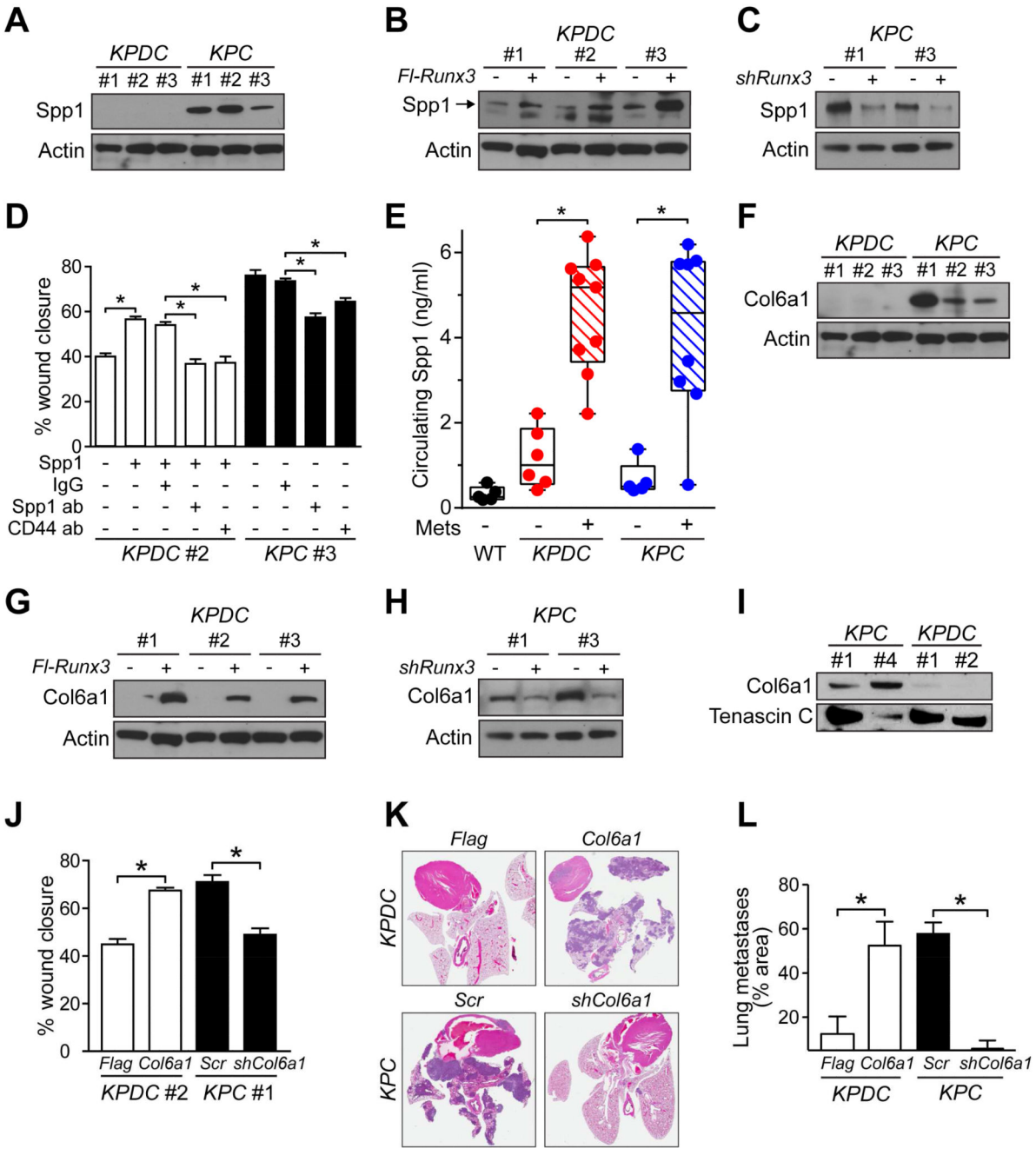

Figure 4. Runx3 stimulates expression of pro-metastatic ECM components

(A) Immunoblots for Spp1 in *KPDC* and *KPC* primary PDA cells.

(B) Immunoblots for Spp1 in control (−) and *Runx3*-overexpressing (+) *KPDC* cells.

(C) Immunoblots for Spp1 in control (−) and *Runx3*-knockdown (+) *KPC* cells.

(D) *KPDC* and *KPC* primary carcinoma cell migration under the indicated conditions, representative of 3 independent experiments (mean ± SEM; *p<0.001).

(E) Circulating Spp1 in *KPC* and *KPDC* animals with (+) or without (−) metastatic disease. Points represents the mean of duplicate measurements from mice (*p<0.005).

(F) Immunoblots for Col6a1 in independent *KPDC* and *KPC* primary PDA cell preparations. (Loading control was the same as in (A)).
(G) Immunoblots for Col6a1 in control (*Flag*) and *Runx3*-overexpressing (*Flag-Runx3*) *KPDC* cells. (Loading control was the same as in (B)).
(H) Immunoblots for Col6a1 in control (−, *Scr*) and *Runx3*-depleted (+, *shRunx3*) *KPC* cells. (Loading control was the same as in (C)).
(I) Col6a1 immunoblots of conditioned media from *KPC* and *KPDC* cell lines. Tenascin C, loading control.
(J) *KPDC* and *KPC* primary carcinoma cell migration +/− Col6a1 overexpression (*Col6a1*) or depletion (*shCol6a1*), respectively. Mean ± SEM of 3 independent experiments (*p<0.0001).
(K) Representative lung sections from mice injected i.v. with either depleted or overexpressed *Col6a1* in *KPC* and *KPDC* cells, respectively (n=2 cell lines and 3 animals for each condition).
(L) Quantification of metastatic pulmonary tumor burden from assays in (K). Two different histological levels from a total of three injected animals were assessed (mean ± SEM; *p<0.05).
See also Figure S4.

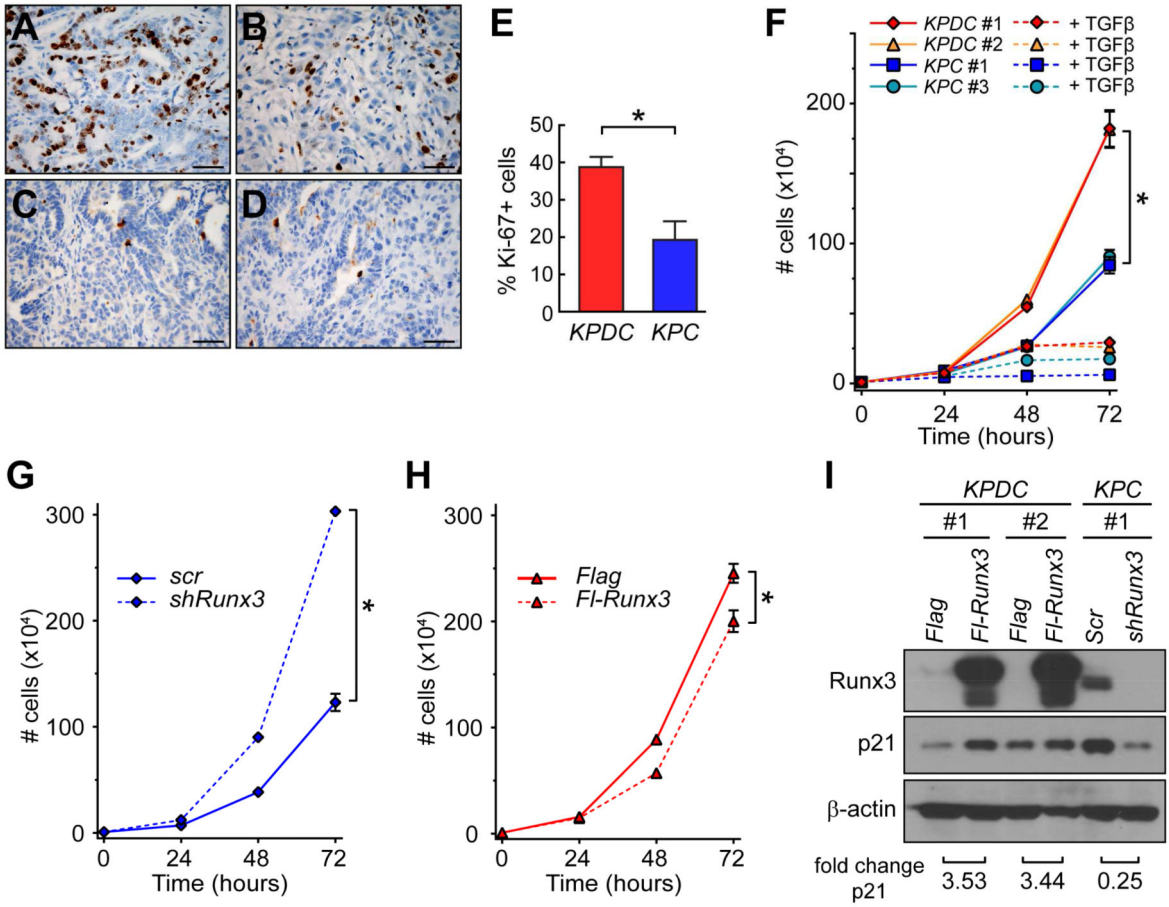

Figure 5. Runx3 inhibits proliferation in invasive PDA cells

(A and B) Ki-67 expression in autochthonous (A) *KPDC* and (B) *KPC* PDA.

(C and D) Cleaved caspase 3 in autochthonous (C) *KPDC* and (D) *KPC* PDA.

(E) Proliferation in autochthonous *KPDC* and *KPC* tumors (mean ± SEM, *p<0.05).

(F) Proliferation of purified PDA cells ±TGFβ *in vitro* (n=3, mean ± SEM; *p<0.001).

(G) Proliferation of control (*Scr*) and *Runx3*-knockdown (*shRunx3*) purified primary *KPC* cells *in vitro* (n=3, mean ± SEM; *p<0.001).

(H) Proliferation of control (*Flag*) and Runx3-overexpressing (*Fl-Runx3*) purified *KPDC* cells *in vitro* (n=3, mean ± SEM; *p<0.001).

(I) Immunoblots for p21 in control and *Runx3*-overexpressing *KPDC* cells and control and *Runx3*-depleted *KPC* cells. Fold changes were quantified by densitometry and normalized to actin. Scale bars, 50 μm.

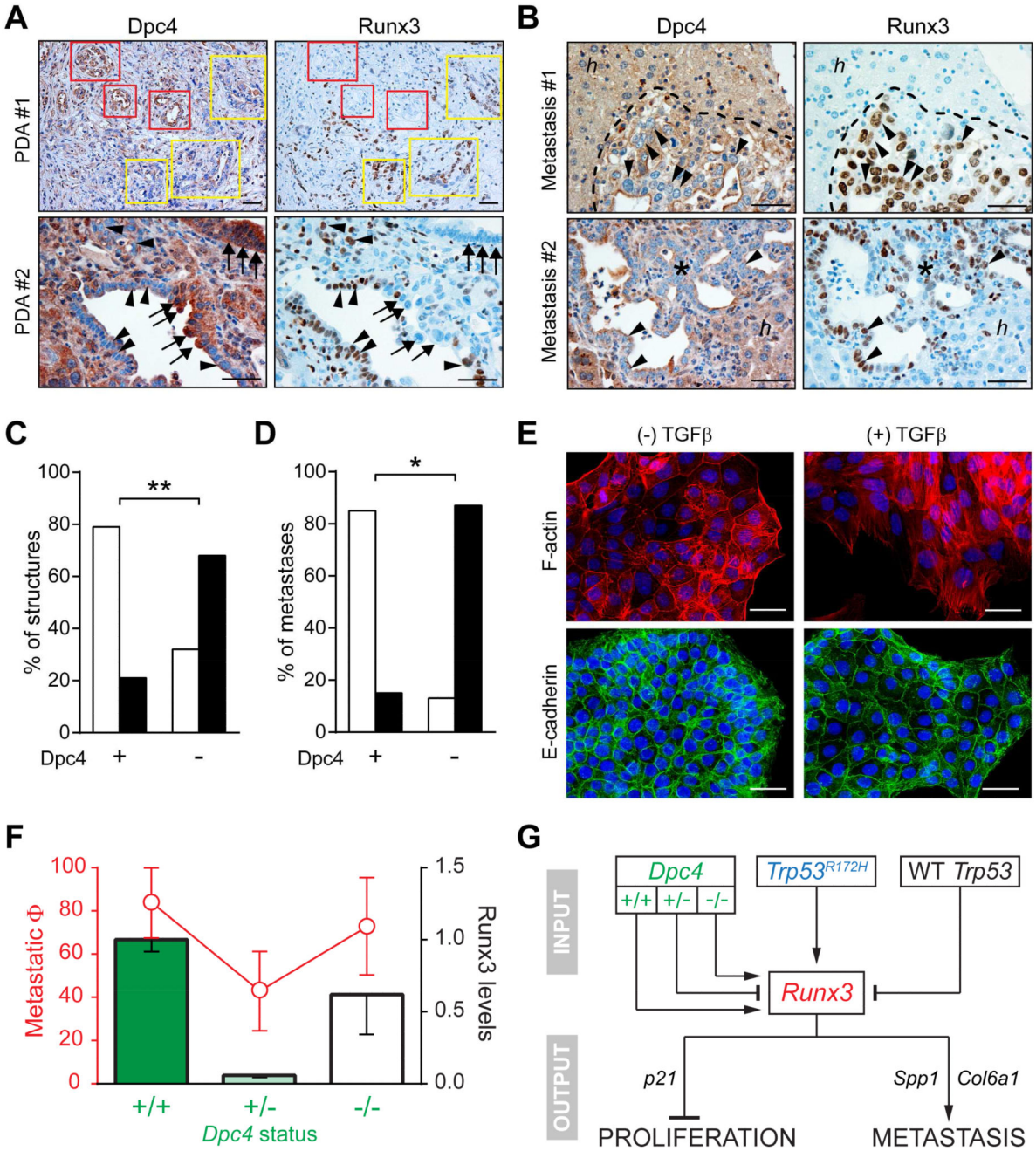

Figure 6. *Dpc4* and *Runx3* coordinately regulate metastatic behavior in PDA

(A) Spontaneous focal loss of Dpc4 (left) in representative autochthonous *KPDC* PDA correlates with acquired Runx3 expression (right). Yellow boxes and arrowheads indicate areas of focal Dpc4 loss and acquired Runx3 expression in tumor epithelia; red boxes and arrows indicate regions of Dpc4 retention and undetectable Runx3.

(B) Liver metastases (asterisks and dotted outlines) from *KPDC* mice reveal spontaneous loss of Dpc4 and corresponding increases in Runx3 expression (arrowheads). Note that hepatocytes (*h*) retain Dpc4 and do not express Runx3.

(C and D) Quantification of Dpc4 and Runx3 IHC in (C) glandular structures in primary *KPDC* tumors and (D) liver metastases from *KPDC* mice. Runx3-low structures/metastases are represented by open bars and Runx3-high by black bars. Fisher's exact test revealed a significant correlation between Dpc4 loss and Runx3 expression (**p<0.0005, *p<0.005).
(E) Immunofluorescence of actin stress fibers (upper panels) and surface E-cadherin (lower panels) in *KPDDC c*ells ±TGFβ. Nuclei are counterstained with DAPI (blue).
(F) Metastatic potential (Φ) plotted as fraction of mice exhibiting metastases (red, ± 95% confidence interval) and relative Runx3 protein levels (black outlined bars; mean ± SEM) as a function of *Dpc4* status (green).
(G) Model for the regulation and role of Runx3 in proliferation and metastasis of PDA. *Runx3* levels are influenced by *Dpc4* status in a biphasic manner and increase only after LOH of *Trp53* in the context of point-mutant *Trp53*. *Runx3* expression in turn stimulates synthesis and secretion of proteins that promote migration and metastatic niche preparation, while simultaneously inhibiting proliferation.
Scale bars, 50 μm. See also Figure S5.

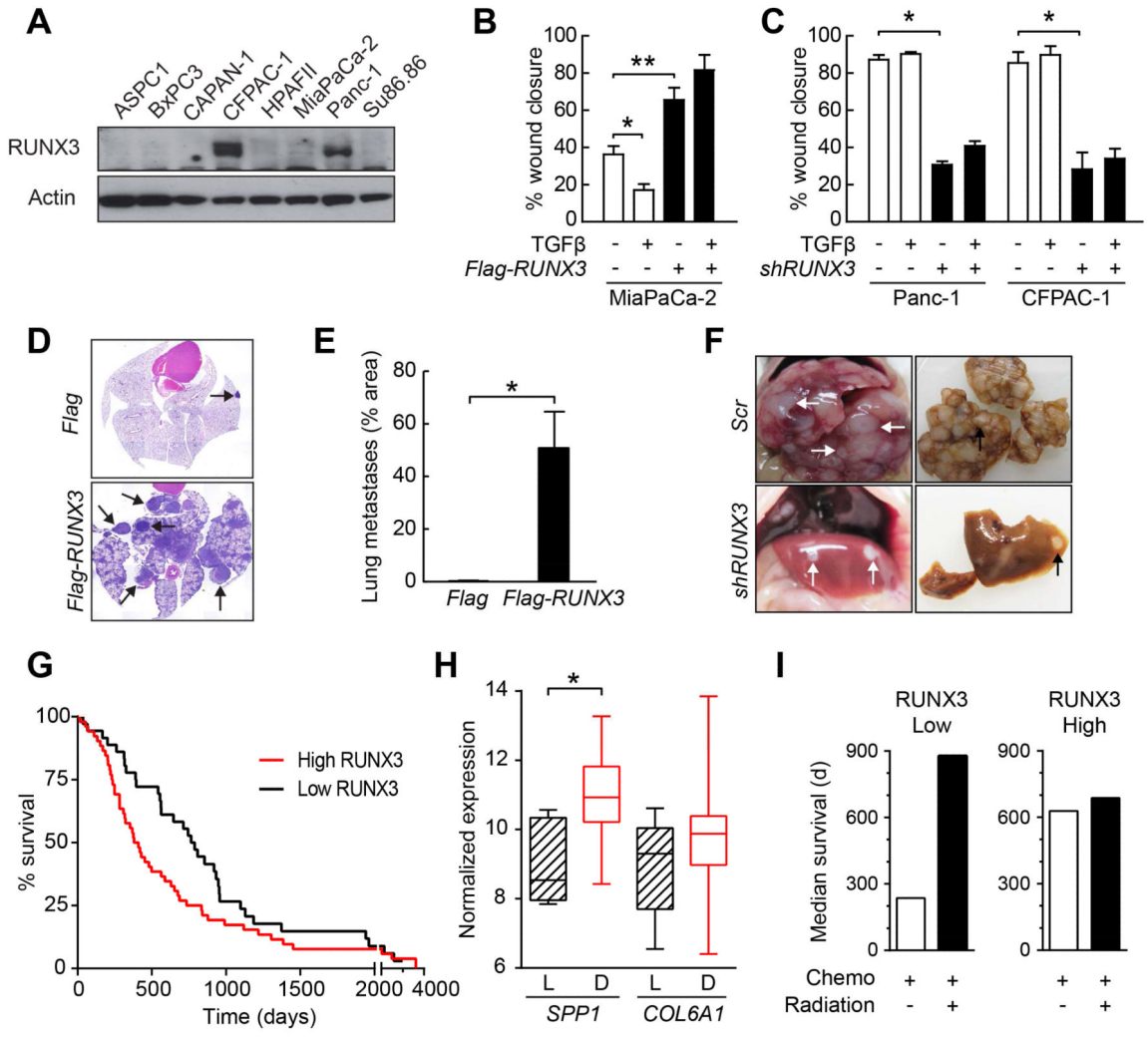

J

Marker		Proximal Risk		Recommended Therapy	
RUNX3	DPC4	Local	Distant	Neoadjuvant	Adjuvant
HIGH	Present	++	+++	Chemo	Chemo
HIGH	Absent	++++	+++	Resect[1]	Chemo + RT
LOW	Present	+++	+	Resect	RT

Figure 7. RUNX3 promotes metastasis in human PDA

(A) Immunoblots for RUNX3 in human PDA lines.

(B) Migration of control (*Flag*) and *RUNX3*-overexpressing (*Flag-RUNX3*) MiaPaCa-2 cells ±TGFβ (n=3, mean ± SEM, *p<0.05, **p<0.01).

(C) Migration of control (*Scr*) or *RUNX3*-knockdown (*shRUNX3*) Panc-1 and CFPAC-1 cells ±TGFβ (n=3, mean ± SEM, *p<0.01).

(D) Representative lung sections from NOD/SCID mice injected with control (*Flag*) or *RUNX3*-overexpressing (*Flag-RUNX3*) MiaPaCa-2 cells. Arrows, metastases.

(E) Quantified metastatic pulmonary tumor burden from assays in (D). Two histological levels from three injected animals were assessed (mean ± SEM; *p<0.05).
(F) Livers *in vivo* (left) and *ex vivo* (right) from NOD/SCID animals injected with control (*Scr*) or *RUNX3*-knockdown (*shRUNX3*) Panc-1 cells. Arrows, metastases.
(G) Kaplan-Meier survival of patients after resection of a primary pancreas cancer. RUNX3 IHC of the primary tumor was used to stratify patients into high (score≥2; n=52) or low (score<2; n=36) populations; median survivals were 395 and 776 days, respectively (Wilcoxon p<0.018).
(H) ICGC gene array data for *SPP1* and *COL6A1* expression in PDA patients who experienced distant (D; n=39) vs. local (L; n=8) relapse after surgery (*p<0.001; p=0.14, *COL6A1* comparison).
(I) Median survivals in patients (n=24) who received adjuvant systemic treatment with or without local radiation therapy as a function of RUNX3 status (low, score≤2; high, score>2).
(J) RUNX3 and DPC4 levels coordinately help inform clinical decision-making for resectable PDA. These considerations are exploratory and not intended as proscriptive advice. Future prospectively collected information, perhaps augmented with retrospective analyses, will be essential to substantiate, revise or reject this working framework.
[1]An alternative would be a short course of radiotherapy followed by chemotherapy.
See also Figure S6.